energies

MDPI

Article

A Triple-Layer Membrane with Hybrid Evaporation and Radiation for Building Cooling

Mingran Mao [1], Chunzao Feng [1], Junxian Pei [2,*], Huidong Liu [1] and Haifeng Jiang [1,*]

[1] MOE Key Laboratory of Hydraulic Machinery Transients, School of Power and Mechanical Engineering, Wuhan University, Wuhan 430072, China
[2] State Key Laboratory of Hydraulics and Mountain River Engineering, College of Water Resource & Hydropower, Sichuan University, Chengdu 610065, China
* Correspondence: jxpei@scu.edu.cn (J.P.); hfjiang@whu.edu.cn (H.J.)

Abstract: Passive cooling for thermal comfort improvement has received extensive attention for its low energy consumption. However, most of the existing passive cooling technologies require a complex system design and supporting equipment, since they cool the ambient air. Herein, we propose a hybrid evaporative and radiative cooling membrane with a hygroscopic hydrogel sandwiched by two layers of a porous polyethylene aerogel (PEA). The hydrogel implements evaporative cooling. Combining the high solar reflection of PEA and the high infrared emissivity of hydrogel, this hybrid membrane also possesses radiative cooling. In addition, the high infrared transmittance and low thermal conductivity of PEA allow direct heat transfer between the hydrogel and human body, instead of the ambient air. Through comparative experiments and theoretical calculations, it is indicated that the net cooling power delivered by the hybrid membrane to the human body is up to 78.45 W m^{-2}, which is much higher than that of conventional radiative cooling materials. Outdoor demonstration shows that emission below the hybrid membrane can achieve an average sub-ambient temperature drop of 6 °C, with a maximum of 14 °C, showing great potential for passive building cooling and human personal cooling.

Keywords: building cooling; radiative cooling; evaporative cooling; passive cooling; polyethylene aerogel

Citation: Mao, M.; Feng, C.; Pei, J.; Liu, H.; Jiang, H. A Triple-Layer Membrane with Hybrid Evaporation and Radiation for Building Cooling. *Energies* **2023**, *16*, 2750. https://doi.org/10.3390/en16062750

Academic Editor: Boris Igor Palella

Received: 8 February 2023
Revised: 2 March 2023
Accepted: 13 March 2023
Published: 15 March 2023

1. Introduction

Mainly affected by greenhouse gas emissions, Earth's average surface temperature is gradually increasing, known as global warming, and local regions will suffer from extreme heat. Air conditioning has become the most common approach to improve human thermal comfort for preventing high temperatures [1,2]. It was projected that the global stock of air conditioners in buildings will grow to 5.6 billion by 2050 [3]. However, large-scale deployment and long-term operation of air conditioners will in turn create more greenhouse gas emissions because of their high energy consumption and refrigerant usage [4–8], thereby exacerbating global warming. Due to the lack of necessary ventilation, air quality in air-conditioned rooms would decline over time, which could cause health issues such as headache [9], nasal congestion [10], and skin diseases [11]. With escalating concerns over environmental threats and health hazards, tremendous efforts to pursue sustainable thermal comfort management technology [12,13] have been made in the past decades, and even more are required currently.

Passive cooling technology [14] without electricity input has attracted considerable attention, and been considered as a promising solution to breaking the vicious cycle between greenhouse gas emissions and increasing demand for cooling. Common passive methods include ventilation [15–17], evaporative cooling [18], radiative cooling [19–22], etc. Ventilation methods utilize the air pressure difference between buildings and the

surrounding environment to increase the convective heat transfer coefficient [23]. Excellent ventilation can improve thermal comfort to some extent, but requires full consideration of sunlight orientation, location, and climate conditions when the building was designed, which is complex and not universal [24,25]. Evaporative cooling methods that dissipate heat through water evaporation could effectively reduce the temperature, but water supply accessories complicate the system [26,27]. Radiative cooling can be enabled by coatings, but its cooling power (with a thermodynamic limitation of about 150 W m^{-2}) often depends on regions and weather conditions [28,29]. Thus, this method is usually coupled with other cooling technologies. For example, radiative cooling could be adopted to cool the water in fluid cooling panels integrated on buildings to increase heat dissipation [30], and it could also be thermally coupled with conventional air conditioners to reduce the energy consumption [31]. These methods all cool the human body by cooling the fluid first, and then lowering the indoor air temperature through heat exchange, which further increases the complexity of the system. Recently, the combination of radiative cooling and evaporative cooling with a bilayer porous polymer has been demonstrated to reach a remarkable cooling effect. They all realize the high cooling capacity by combining radiative cooling materials and hydrogels, but none of them paid attention to heat loss from the surrounding environment [32–34]. Another type of material that uses the synergy effect of radiative cooling and evaporative cooling is passive daytime cooling fabrics [35,36]. They can directly cool the human body, but because the fabric itself can only cover part of the human body, the cooling effect it brings is limited. Some scholars also use the infrared transparency and low thermal conductivity of aerogel to reach a lower cooling temperature [37]. Nonetheless, the problem of ambient heat leakage caused by indoor ambient air being cooled is still unsolved, and these designs are all aimed at cooling the human body by reducing the surface temperature of the building. Therefore, there is still an urgent need to develop a simple and efficient cooling method to both avoid ambient heat leakage and directly cool the human body.

Here, we propose a PEA-hydrogel-PEA (PHP) composite membrane that integrates radiative cooling and evaporative cooling, which can directly exchange heat with the human body. As shown in Figure 1, the upper and lower PEA layers are highly reflective in the solar spectrum, and highly transparent in the mid-infrared spectrum. The middle hydrogel layer has a high infrared emissivity, which can not only absorb heat from the high temperature human body, but can also dissipate the absorbed heat by evaporating water to the environment and radiating electromagnetic waves into outer space. The low thermal conductivity of PEA can better prevent the input of ambient heat compared with traditional radiative cooling materials. Furthermore, ion-treated hydrogel that evaporates at high temperatures and regenerates water from air at low temperatures allows for the absence of water supply accessories. By adding a mechanical structure and skeleton support, PHP can be laid outdoors to build a sunshade pavilion or a simple shade house for practical applications. These characteristics demonstrate an effective personal cooling enhancement and a potential application of the PHP membrane for passive building cooling.

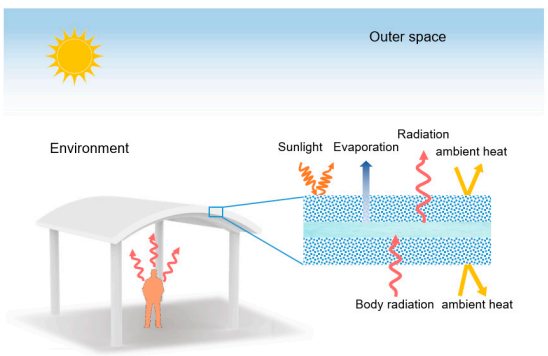

Figure 1. Schematic of the proposed triple-layered membrane.

2. Materials and Methods

2.1. Preparation of PEA

Polyethylene aerogel was prepared by thermal phase separation and critical point drying methods [37,38]. Firstly, 98.5 wt% high density paraffin oil, 1 wt% ultra-high molecular weight polyethylene (UHMWPE), and 0.5 wt% butylated hydroxytoluene were mixed in a sealed beaker, which was put into a 160 °C oil bath and stirred for half an hour. After stirring, the mixture was poured into an aluminum mold. Then, the model was placed horizontally in an ice bath to obtain the polymer gel. The paraffin oil in the polymer gel was subsequently extracted by hexane, and the hexane was extracted by ethanol. Finally, the PEA sample was obtained after the ethanol in the polymer gel was dried in a critical point dryer (E3100-060, Quorum Technology, Lewes, UK).

2.2. Preparation of Ion-Treated Hydrogel

Hydrogel was fabricated by the photopolymerization method [39], starting with a mixed solution with 2 mol L^{-1} acrylamide monomer (AAm), 0.001 mol L^{-1} N,N′-methylenebisacrylamide, and 0.002 mol L^{-1} 2-hydroxy-4′-(2-hydroxyethoxy)-2- methylpropiophenone. Then, an acrylic mold was filled with the mixed solution and irradiated by an ultraviolet lamp with a power density of ~4 mW cm^{-2} for the phtotopolymerization process of the PAAm hydrogel under a nitrogen atmosphere. After that, the PAAm hydrogel was completely dried in an oven at 60 °C. Finally, the dried PAAm hydrogel was put into a 30 wt% LiBr solution until it was fully swollen to obtain the ion-treated hydrogel, or Li-hydrogel.

2.3. Assembly of PHP Membrane

The prepared PEA and Li-hydrogel were cut into the same size and stacked in layers to obtain the PHP composite membrane, with the upper and lower layers of PEA, and a middle layer of hydrogel.

2.4. Characterizations

The morphologies of PEA samples and dry hydrogel samples were characterized by scanning electron microscopy (TESCAN, MIRA 3). A Fourier infrared spectrometer (FTIR, INVENIO S, Bruker) was used to measure the mid-infrared spectrum of samples, and a UV-Vis-NIR spectrophotometer (Lambda 1050, Perkin Elmer) was used to measure the samples' spectra in the visible and near-infrared bands. The thermal conductivity of PEA and P(VdF-HFP) samples was measured using a thermal conductivity meter (TC3000E, XIAXI).

2.5. Outdoor Cooling Performance Measurements and Demonstration

We recorded the solar intensity by using an optical power meter (CELNP2000-2), and monitored the environment's real relative humidity by using a thermo-hygrometer (CENTER 310). Temperatures were recorded by using thermocouples (TT-K-30, Omega Company) and a data logger (TC-08, Pico Technology). Mass changes of Li-hydrogel were recorded by using an electronic balance (ML-T, Mettler Toledo).

2.6. Measuring Heat Transfer Performance of PEA

To measure the radiative cooling power through different PEA thicknesses, we kept the heater at ~36 °C using a TEC thermostat (TCM1030, YEXIAN), and the whole experiment setup was placed in an incubator at 36 °C. We used a water bath (DC-3010, SHUNMA) to keep the cold end at different low temperatures. At different water bath temperatures, the radiative cooling power delivered to the heater through PEA was different, resulting in different input voltages of the heater. The voltages of the heater were recorded by a source meter (Keithley 2000). Temperatures were recorded by thermocouples (TT-K-30, Omega Company) and a data logger (TC-08, Pico Technology).

2.7. Calculations

The net cooling power ($P_{cool,net}$) of the samples was calculated by the evaporation cooling power (P_{eva}), the radiation cooling power (P_{rad}), the absorbed solar power (P_{sun}), and the ambient convection power (P_{amb}):

$$P_{cool,net} = P_{eva} + P_{rad} - P_{sun} - P_{amb}, \quad (1)$$

The evaporation cooling power was estimated by:

$$P_{eva} = \frac{\Delta H \times \Delta m}{t \times A}, \quad (2)$$

where ΔH is the enthalpy of water vaporization (2260 J g^{-1}), t is evaporation time, Δm is the weight loss, and A is the evaporation area of the hydrogel.

The radiation cooling power was described by [32]:

$$P_{rad} = \tau_{air} \int_{8\mu m}^{14\mu m} U_B(T_s, \lambda)\varepsilon_s(\lambda, \theta)d\lambda, \quad (3)$$

$$e_s = \frac{\int_{8\mu m}^{14\mu m} U_B(T_s, \lambda)\varepsilon_s(\lambda, \theta)d\lambda}{\int_{8\mu m}^{14\mu m} U_B(T_s, \lambda)d\lambda}, \quad (4)$$

$$\tau_{air} = \frac{\int_{8\mu m}^{14\mu m} U_B(T_a, \lambda)\tau_a(\lambda, \theta)d\lambda}{\int_{8\mu m}^{14\mu m} U_B(T_a, \lambda)d\lambda}, \quad (5)$$

where τ_{air} is the average atmospheric transmittance. T_s and T_a are temperatures of sample and ambient air, respectively. $U_B(T, \lambda)$ is the spectral radiance of a black body. $\varepsilon_s(\lambda, \theta)$ is the emissivity of sample and e_s is the average spectral emissivity in 8–14 µm. $\tau_a(\lambda, \theta)$ is the atmospheric transmittance modeled by MODTRAN® 6.

The absorbed solar power was calculated by [32]:

$$P_{sun} = I_{solar} \times (1 - r_{sun}), \quad (6)$$

$$r_{sun} = \frac{\int_{0.3\mu m}^{2.5\mu m} U_B(T_s, \lambda)r_s(\lambda, \theta)d\lambda}{\int_{0.3\mu m}^{2.5\mu m} U_B(T_s, \lambda)d\lambda}, \quad (7)$$

where I_{solar} is the incident solar power and r_{sun} is the average spectral reflectance in 0.3–2.5 µm. $r_s(\lambda, \theta)$ is the reflectance of the sample. PHP can be regarded as a gray body and the spectral absorption ratio of PHP material does not vary with wavelength.

The ambient convection power was calculated by:

$$P_{amb} = h \times \Delta T, \quad (8)$$

where the h is the convection coefficient, which was estimated using the wind speed V and from an empirical equation $h = 2.8 + 3.0V$ for forced convection over a flat plate [40]. Local wind speed on the day of the experiment was about 3.6 m s^{-1}. ΔT is the temperature difference between the sample surface and the environment.

3. Results and Discussion

Figure 2a shows the structure of the PHP membrane with hydrogel sandwiched by two layers of PEA. The upper PEA layer has slanted holes with a diameter of ~1 mm (inset on the top right) to accelerate the evaporation of the hydrogel. A SEM image of the hydrogel shows a porous structure with a pore size of ~20 µm. The porous features and polymer chains of the hydrogel allow it to have a water content of up to 98%, and the addition of Li+ makes it environmentally adaptable. As shown in Figure 2b, a piece of

Li-hydrogel with 30 wt.% LiBr continuously keeps evaporating at an ambient temperature of ~36 °C and relative humidity of 55%, and starts to absorb water when cooled to ~26 °C, until it returns to its original weight. The self-adaptability of the Li-hydrogel enables the PHP membrane to achieve evaporative cooling at a high temperature, and automatic water replenishment when cooled. A great number of micropores smaller than 1 µm was observed in the PEA sample as well (Figure 2a), indicating that PEA layers mainly exhibit Rayleigh scattering in the mid-infrared spectrum, with high transmittance and Mie scattering in the visible and near-infrared bands with a high reflectance. Figure 2c shows the reflectance and transmittance of PEA in a wavelength range from 0.3 µm to 25 µm. According to Equation (7), the solar reflectance of PEA samples with a 2 mm, 4 mm, and 6 mm thickness are calculated as 0.962, 0.957, and 0.968, respectively. Their transmittances are 0.863, 0.763, and 0.685, respectively, within the atmospheric spectral window, according to Equation (5). Notably, the infrared emissivity of PHP is ~0.89, due to enhancement of the high emissive hydrogel layer (Figure S1). Combined with the high solar reflectance of the PEA layer, the hybrid membrane can serve as a typical radiative cooling material. Moreover, owing to its porous structure, PEA has a low thermal conductivity of ~3.07 W cm^{-1} K^{-1} (Figure 2d), which can effectively reduce heat exchange between the hybrid membrane and ambient air.

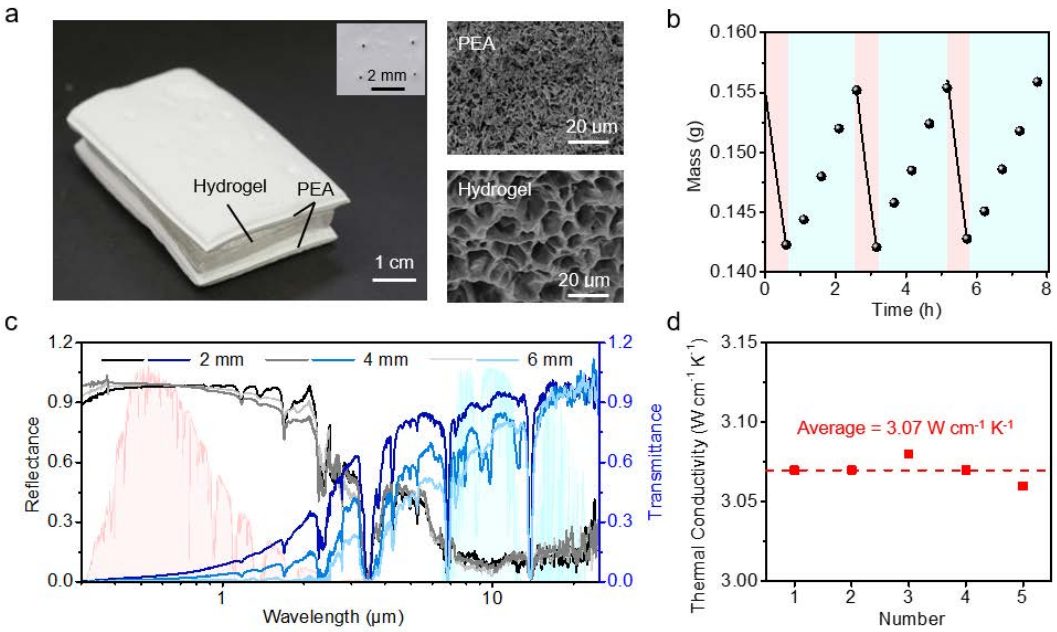

Figure 2. Structure and characterizations of the PHP membrane. (**a**) Photograph of a PHP membrane with a size of ~4 cm × 6 cm. SEM images of a PEA sample (**top right**) and hydrogel sample (**bottom right**). (**b**) Mass changes of a hydrogel (~4 cm × 1 cm × 0.5 cm) during repeating evaporation and regeneration processes. (**c**) Hemispherical transmittance and reflectance of the 2 mm PEA, 4 mm PEA, and 6 mm PEA samples, along with the normalized AM 1.5 solar spectrum, and the transparent atmospheric window in the mid-infrared spectrum. (**d**) Thermal conductivity of a PEA sample.

In order to investigate the cooling performance of the hybrid membrane, we conducted outdoor experiments under direct sunlight with four groups of samples, including PEA and hydrogel, PEA and emitter (black polyvinyl chloride), poly (vinylidene fluoride-co-hexafluoropropene) [P(VdF-HFP)], and stainless steel. The schematic and photograph of the setup are shown in Figure 3a and Figure S2, respectively. The thickness of the PEA layer was chosen to be 6 mm due to its high insulating performance according to theoretical calculations (Figure S3). Considering that the heat on the lower surface of the P(VdF-HFP) needs to be conducted to the upper surface for radiative cooling, 3 mm thick P(VdF-HFP) is used here. Thermocouples were placed at the interface of the PEA and hydrogel (T_1), the interface of the PEA and emitter (T_2), the lower surface of the PVDF (T_3), and the

lower surface of the stainless steel sheet (T_4) to measure the cooling temperature of each group of samples. Another thermocouple was placed in a ventilated place not exposed to direct sunlight for measuring ambient temperature (T_5). Figure 3b shows the outdoor measurements in Wuhan with a sunlight intensity of ~69.32 mW cm^{-2} and ambient relative humidity of ~44%. The average temperature of the PEA and hydrogel can be as low as 6.3 °C below ambient, with a continuous mass loss of the hydrogel. A sub-ambient temperature drop of 4.2 °C, on average, can also be achieved for the PEA and emitter with a pure radiative cooling effect. The solar reflectance and thermal emissivity of the PEA and hydrogel are almost the same as those of the PEA and emitter, with a reflectivity of 0.97 and 0.968, respectively, and emissivity of 0.89 for both (Figure S4). The significant temperature drop of the PEA and hydrogel demonstrates the dual-effect of radiative and evaporative cooling. Comparatively, P(VdF-HFP) [41], a common radiant cooling material, performs an average temperature drop of only 2.6 °C, even though its reflectivity in the solar wavelength range and emissivity in the atmospheric window are 0.94 and 0.935, respectively. As an actual building material, stainless steel has a solar reflectivity of 0.599 and an atmospheric window emissivity of 0.3, and its temperature is 8.5 °C higher than the ambient temperature.

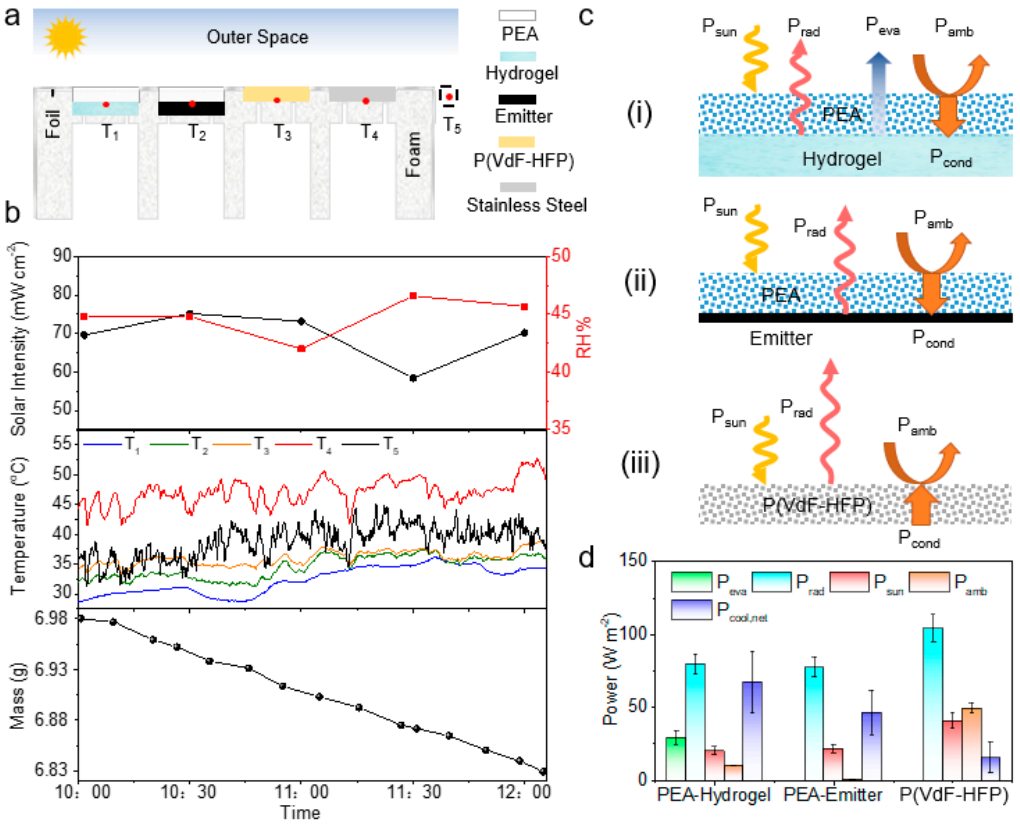

Figure 3. Cooling performance of the PEA and hydrogel membrane. (**a**) Schematic of the experimental setup. (**b**) Outdoor experiment from 10:00 to 12:10 14 Jun 2022 in Wuhan, China. Top panel: real-time solar intensity and environment humidity; middle panel: temperatures of the PEA and hydrogel sample (blue line, T_1), the PEA and emitter sample (green line, T_2), the P(VdF-HFP) sample (orange line, T_3), the stainless steel substrate (red line, T_4) and the environment (black line, T_5); bottom panel: mass changes of the hydrogel (4 cm × 4 cm × 4 mm, 30 wt% LiBr). (**c**) Heat transfer models of the PEA and hydrogel (**i**), the PEA and emitter (**ii**) and the P(VdF−HFP) (**iii**). (**d**) Average evaporative, radiative, net cooling, absorbed solar, and ambient convection power of the PEA and hydrogel sample, the PEA and emitter sample, and the P(VdF-HFP) sample.

To evaluate the thermal insulation enhancement of the PEA, heat transfer of the PEA and hydrogel, the PEA and emitter, and the P(VdF-HFP) are analyzed through the models in Figure 3c. For the PEA and hydrogel, the input energy consists of the solar absorption and convective heat transfer between the ambient air and the upper surface of the PEA, while the output energy should include the radiant heat from the hydrogel to outer space through the PEA, and evaporative heat dissipation to the ambient air. Due to thermal radiation of the emitter, the lower surface of the PEA will be cooler than the upper surface, which will result in heat conduction from the top to the bottom within the PEA (Figure 3c(i)). The evaporative component should be excluded for the PEA and emitter (Figure 3c(ii)). Different from the PEA and hydrogel and the PEA and emitter, the thermal radiation of the P(VdF-HFP) is emitted from the upper surface, thus resulting in heat conduction from the bottom to the top (Figure 3c(iii)). Figure 3d shows the power components of different heat transfer processes. Clearly, heat transfer from the environment to the emitter/hydrogel with the PEA is much lower than that of conventional radiative cooling materials, such as P(VdF-HFP). The extremely high P_{amb} of P(VdF-HFP) originates from direct contact between its upper surface and the hot air. The ambient heat transfer of the PEA and hydrogel is higher than that of the PEA and emitter because of the lower hydrogel temperature, but its cooling power is still increased by ~40% due to the evaporative cooling of the hydrogel, with the $P_{cooling,net}$ of the PEA and hydrogel and the PEA and emitter being 78.45 W m^{-2} and 56.08 W m^{-2}, respectively. Although the P_{rad} of P(VdF-HFP) is the highest, its $P_{cooling,net}$ is only 14.61 W m^{-2} because of the higher P_{sun} and P_{amb}, and its low thermal conductivity of ~4.22 W cm^{-1} K^{-1} (Figure S5).

In order to verify direct heat exchange between the hydrogel and the human body through the PEA, we conducted indoor experiments with a setup as shown in Figure 4a. An emitter, temperature-controlled by a thermostatic water bath, was used instead of a hydrogel as a cold plate, under which the PEA was covered to reduce its heat exchange with the environment. A heater was used to simulate the surface of human skin, which was controlled by a thermostat to maintain 36 °C. All of them were sealed in thermal insulation foams with distance of 4 cm between the heater and emitter. The whole experimental setup was placed in a 36 °C thermostatic container. In the initial state, the heater had power input. When the temperature of the water bath dropped to 28 °C, 24 °C, 20 °C, 16 °C, and 12 °C, and kept for 1 hour in turn, the voltage of the heater was recorded to calculate its input power (Figure S6). Figure 4b indicates the typical temperature vibrations of the water bath and the 2 mm thick PEA. Due to the constant temperature of the ambient air and the heater, the average input power of the heater, corresponding to different water bath temperatures, can be regarded as the radiative cooling power $P_{rad,body}$ transmitted from the heater (human body) to the water bath through the PEA.

The calculated $P_{rad,body}$ at different water temperatures is shown in Figure 4c, the largest of which is the no-PEA sample, followed by the ones with 2 mm, 4 mm, and 6 mm PEA. It is clear that the $P_{rad,body}$ decreased slightly with the PEA thickness at the same water temperature. When the water temperature approaches the ambient temperature, the effect of the PEA layer on the $P_{rad,body}$ become smaller. In addition to the radiative cooling power $P_{rad,body}$, there is also part of the cooling power to the environment through heat conduction of the PEA layer, labeled as P_{con}. According to the temperatures on the upper and lower surfaces of the PEA, and the thermal conductivity of the PEA, the P_{con} at different water temperatures can be calculated as shown in Figure 4d. The lower thermal conductivity of the PEA results in a significant reduction of the P_{con}, and the reduction rate becomes more obvious with the increase of the PEA thickness, reaching a maximum of 68% at 6 mm thick PEA. Here, we define a new constant $\eta = \frac{P_{rad,body}}{P_{rad,body}+P_{con}}$ to characterize the relative intensity of radiative cooling, which represents the proportion of radiative cooling power in the total cooling power with the water bath or hydrogel. As shown in Figure 4e, η is not significantly affected by the water temperature, but is greatly affected by the PEA thickness. Due to the thermal insulation enhancement, samples with 6 mm thick PEA have the highest η value, indicating a larger direct-to-body cooling capacity under the same conditions.

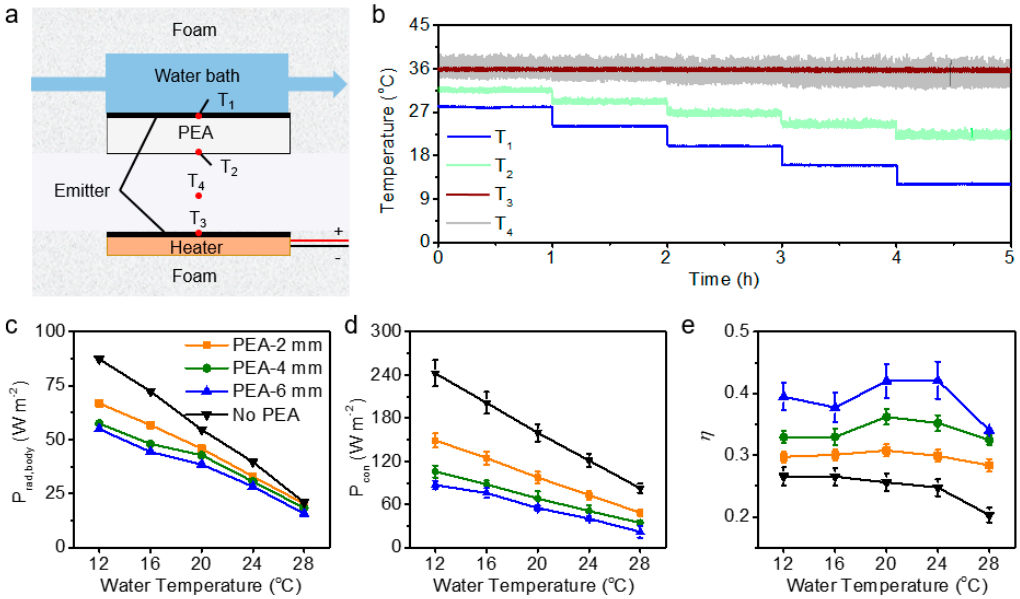

Figure 4. Heat transfer performance of the PEA samples. (**a**) Schematic of the experimental setup. (**b**) Temperatures recordings of the 2 mm thick PEA top surface (green line, T_2), the heater (red line, T_3), and ambient (gray line, T_4) in different water bath temperatures (blue line, T_1). (**c**,**d**) The radiative power from the heater (**c**) and conduction power from the environment (**d**) to the water bath at different temperatures with different thickness PEA samples. (**e**) The ratio (η) of radiative power to conduction power with different water bath temperatures.

According to the results of the indoor and outdoor experiments, a hybrid PHP membrane with both upper and lower PEA of 6 mm thickness was prepared for outdoor demonstration. The schematic diagram and photograph of the experimental setup are shown in Figure 5a,b. Here, an emitter was placed inside a thermally insulating foam box with inner dimensions of 30 cm × 30 cm × 20 cm. The outer surface of the foam is affixed with tin foil to prevent the entry of sunlight. A square hole, with 4 cm × 6 cm on the top of the box, is covered by a piece of the PHP membrane for heat exchange between the emitter and the outside world. The emitter is 2 cm away from the lower surface of the PHP. Under these conditions, the cooling capacity delivered to the body can be assessed by the emitter surface temperature. Another PHP membrane, with a foil film between the hydrogel and underlying PEA, labeled as PHP-foil, and stainless steel with a layer of black polyvinyl chloride on the back, are set as controls. The foil film could block radiative heat transfer between the PHP and the emitter. The spectra of the emitter and the PEA on foil are shown in Figure S7. The demonstration was conducted under direct sunlight with an intensity above 65 mW cm^{-2} and a relative humidity of ~54.86% (Figure S8). The measured temperature vibrations are shown in Figure 5c. In order to measure the cooling temperature of each group, we placed thermocouples at the interface of the hydrogel and the lower-PEA in the PHP (T_1'), the interface of the hydrogel and the foil in the PHP-foil (T_2'), and the black polyvinyl chloride layer on the stainless steel (T_3'). Another thermocouple was placed in a shaded and ventilated place for measuring the ambient temperature (T_4). T_1, T_2, and T_3 are the temperatures of the emitters under the PHP, PHP-foil, and stainless steel, respectively. Attractively, benefiting from the dual-effect cooling of the PHP membrane, both T_1' and T_2' are much lower than the ambient temperature T_4. Combined with the direct heat exchange between the emitter and the PHP membrane, T_1 can achieve an average sub-ambient temperature of ~6 °C, with a maximum of ~14 °C at around 12:10. In contrast, because the radiative heat exchange between the emitter and the hydrogel is isolated by the foil, T_2 is only ~3 °C below the ambient temperature, although T_2' is the lowest. T_3 is very close to T_4 because T_3' is even higher than the ambient temperature, due to the lack of effective heat dissipation. The results demonstrate that the PHP membrane can realize the

cooling of the membrane itself, and effectively transfer the cooling capacity to the human body at high ambient temperatures.

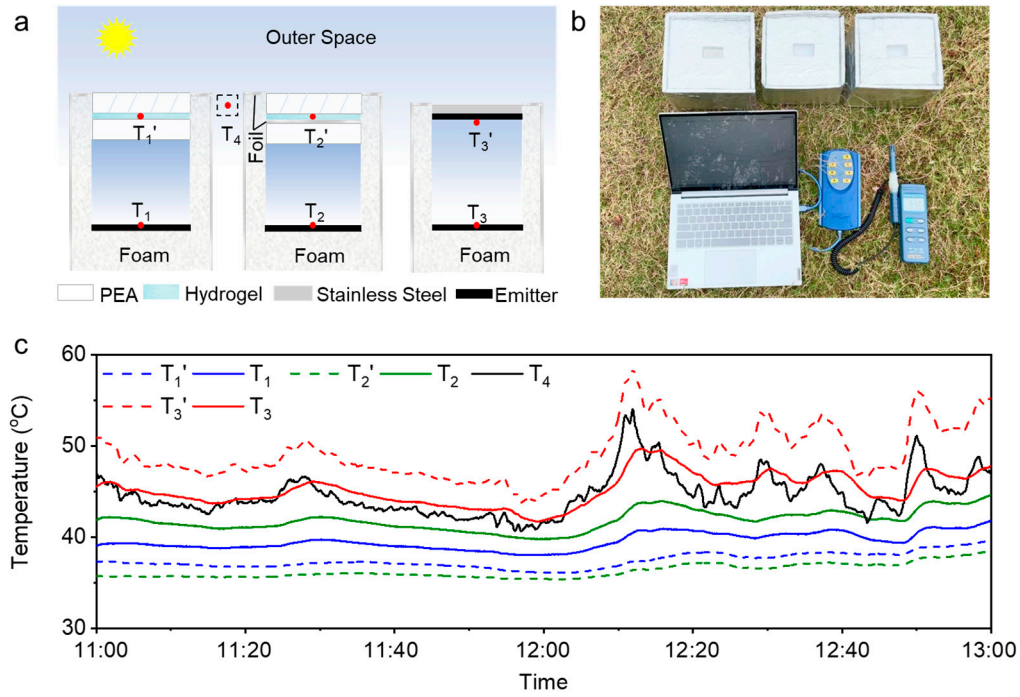

Figure 5. Demonstration of the cooling performance of the PHP membrane in outdoor conditions. (**a**,**b**) Schematic (**a**) and photograph (**b**) of the experimental setup. (**c**) The temperatures of the PHP sample (blue line, T_1 and T_1'), the PHP-foil sample (green line, T_2 and T_2'), the stainless steel sample (red line, T_3 and T_3'), and ambient (black line, T_4) from 11:00 to 13:00 7 July 2022 in Wuhan, China.

4. Conclusions

In summary, we have designed a triple-layer membrane (PHP) that can use passive cooling technology to directly cool the human body at high ambient temperatures. The triple-layer membrane consists of two layers of PEA and a Li-hydrogel layer between them. The infrared transparency of the PEA allows direct heat transfer between the hydrogel and the human body or outer space. Its high solar reflectance and low thermal conductivity can reduce heat absorption from the sun and ambient air. The environment-adaptive hydrogel in the middle can evaporate water to dissipate heat at high temperatures, and absorb water to regenerate at low temperatures. The combination of evaporative and radiative cooling, and avoidance of ambient heat leakage, endow the PHP with a high net cooling power. By establishing a heat transfer model for calculation, we chose 6 mm as the thickness of the upper PEA, which can achieve a net cooling power of about 78.45 W m^{-2} under 69.32 mW cm^{-2} of solar intensity. The radiation heat transfer process of the PHP to the human body was simulated through indoor experiments, and the results show that the relative intensity of the radiative cooling ratio η between the human body and the PHP can reach up to 40%. Through outdoor demonstration, the internal emitter temperature is about 6 °C average lower than that of conventional building materials after using the PHP membrane, and can reach a 14 °C maximum sub-ambient temperature drop, which proves that the PHP can effectively realize the function of direct personal cooling. The described design strategy features a simple structure and efficient heat exchange, showing a great potential in building cooling and thermal controlling.

Supplementary Materials: The following supporting information can be downloaded at: https://www.mdpi.com/article/10.3390/en16062750/s1. Supplementary Materials include Supplementary Notes and Supplementary Figures. Supplementary Notes: 1. Relationship between the PEA thickness

and emitter temperature; 2. The calculation of $P_{cool,net}$. Supplementary Figures: Figure S1: Emissivity of the PHP membrane and hydrogel sample along with the normalized AM 1.5 solar spectrum and the atmospheric transmittance; Figure S2: Photograph of the cooling performance experimental setup; Figure S3: Heat transfer model of the PEA and emitter sample with different thicknesses. (a) Resistance network of the heat transfer between the emitter and ambient air. (b) Absorptivity and extinction coefficient of the PEA samples in the atmospheric window. (c-d) Simulated variation of the emitter temperature with the PEA thickness in different atmospheric transmittance (c) and convective heat transfer coefficients (d); Figure S4: Reflectance spectrum in the AM 1.5 solar spectrum range (a) and emissivity in the infrared range (b) of the PEA and hydrogel sample, the PEA and emitter sample, the P(VdF-HFP) sample, and the stainless steel substrate; Figure S5: Thermal conductivity measurement results of a P(VdF-HFP) sample in five times; Figure S6: Heat transfer experiment of the PEA samples. (a) Temperature recordings of different PEA thicknesses in different water bath temperatures. (b) Voltage that needs to be applied to the heater in order to maintain the same temperature with and without the PEA layer. (c) Corresponding input power of the heater calculated from its voltage and constant 3.5 Ω resistance; Figure S7: Emissivity spectrum of the emitter and the PEA-Foil sample; Figure S8: Real-time solar intensity and environment humidity on 7 July 2022 in Wuhan, China.

Author Contributions: H.L. and H.J. conceived the study; M.M., J.P. and C.F. experimented and carried out theoretical investigations; M.M, C.F., H.L., J.P. and H.J. analyzed the data. All authors contributed equally to writing, editing, and reviewing the manuscript. All authors have read and agreed to the published version of the manuscript.

Funding: J. Pei acknowledges the financial support from Fundamental Research Funds for the Central Universities, Sichuan University under grant number No. YJ2021135.

Data Availability Statement: The authors confirm that the data supporting the findings of this study are available within the article and its supplementary materials.

Conflicts of Interest: The authors declare no conflict of interest.

References

1. Asim, N.; Badiei, M.; Mohammad, M.; Razali, H.; Rajabi, A.; Chin Haw, L.; Jameelah Ghazali, M. Sustainability of Heating, Ventilation and Air-Conditioning (HVAC) Systems in Buildings—An Overview. *IJERPH* **2022**, *19*, 1016. [CrossRef] [PubMed]
2. Tsvetkov, O.B.; Laptev, Y.A.; Sharkov, A.V.; Mitropov, V.V.; Fedorov, A.V. Alternative refrigerants with low global warming potential for refrigeration and air-conditioning industries. *IOP* **2020**, *905*, 012070. [CrossRef]
3. Team, E. *The Future of Cooling: Opportunities for Energy-Efficient Air Conditioning*; International Energy Agency: Paris, France, 2018. [CrossRef]
4. Zhou, C.; Fang, Z.; Xu, X.; Zhang, X.; Ding, Y.; Jiang, X.; Ji, Y. Using long short-term memory networks to predict energy consumption of air-conditioning systems. *Sustain. Cities Soc.* **2020**, *55*, 102000. [CrossRef]
5. Davis, L.W.; Gertler, P.J. Contribution of air conditioning adoption to future energy use under global warming. *Proc. Natl. Acad. Sci. USA* **2015**, *112*, 5962–5967. [CrossRef] [PubMed]
6. Lickley, M.; Solomon, S.; Fletcher, S.; Velders, G.J.M.; Daniel, J.; Rigby, M.; Montzka, S.A.; Kuijpers, L.J.M.; Stone, K. Quantifying contributions of chlorofluorocarbon banks to emissions and impacts on the ozone layer and climate. *Nat. Commun.* **2020**, *11*, 1380. [CrossRef] [PubMed]
7. Kikegawa, Y.; Genchi, Y.; Kondo, H.; Hanaki, K. Impacts of city-block-scale countermeasures against urban heat-island phenomena upon a building's energy-consumption for air-conditioning. *Appl. Energy* **2006**, *83*, 649–668. [CrossRef]
8. Ciconkov, R. Refrigerants: There is still no vision for sustainable solutions. *Int. J. Refrig.* **2018**, *86*, 441–448. [CrossRef]
9. Mendell, M.J.; Smith, A.H. Consistent pattern of elevated symptoms in air-conditioned office buildings: A reanalysis of epidemiologic studies. *Am. J. Public Health* **1990**, *80*, 1193–1199. [CrossRef]
10. Dobson, R. Air conditioned buildings increase risk of sickness. *BMJ* **2004**, *329*, 529. [CrossRef]
11. Chernosky, M.E. Pruritic Skin Disease and Summer Air Conditioning. *JAMA* **1962**, *179*, 1005–1010. [CrossRef]
12. Wang, X.; Li, H.; Sodoudi, S. The effectiveness of cool and green roofs in mitigating urban heat island and improving human thermal comfort. *Build. Environ.* **2022**, *217*, 109082. [CrossRef]
13. Peng, Y.; Chen, J.; Song, A.Y.; Catrysse, P.B.; Hsu, P.-C.; Cai, L.; Liu, B.; Zhu, Y.; Zhou, G.; Wu, D.S.; et al. Nanoporous polyethylene microfibres for large-scale radiative cooling fabric. *Nat. Sustain.* **2018**, *1*, 105–112. [CrossRef]
14. Gupta, N.; Tiwari, G.N. Review of passive heating/cooling systems of buildings. *Energy Sci. Eng.* **2016**, *4*, 305–333. [CrossRef]
15. Laurini, E.; De Vita, M.; De Berardinis, P.; Friedman, A. Passive Ventilation for Indoor Comfort: A Comparison of Results from Monitoring and Simulation for a Historical Building in a Temperate Climate. *Sustainability* **2018**, *10*, 1565. [CrossRef]

16. Suleiman, S.; Himmo, B. Direct comfort ventilation. Wisdom of the past and technology of the future (wind-catcher). *Sustain. Cities Soc.* **2012**, *5*, 8–15. [CrossRef]
17. Campaniço, H.; Hollmuller, P.; Soares, P.M.M. Assessing energy savings in cooling demand of buildings using passive cooling systems based on ventilation. *Appl. Energy* **2014**, *134*, 426–438. [CrossRef]
18. Pearlmutter, D.; Berliner, P. Experiments with a 'psychrometric' roof pond system for passive cooling in hot-arid regions. *Energy Build.* **2017**, *144*, 295–302. [CrossRef]
19. Fan, S.; Raman, A. Metamaterials for radiative sky cooling. *Natl. Sci. Rev.* **2018**, *5*, 132–133. [CrossRef]
20. Zhao, B.; Hu, M.; Ao, X.; Chen, N.; Pei, G. Radiative cooling: A review of fundamentals, materials, applications, and prospects. *Appl. Energy* **2019**, *236*, 489–513. [CrossRef]
21. Lu, X.; Xu, P.; Wang, H.; Yang, T.; Hou, J. Cooling potential and applications prospects of passive radiative cooling in buildings: The current state-of-the-art. *Renew. Sustain. Energy Rev.* **2016**, *65*, 1079–1097. [CrossRef]
22. Ko, B.; Lee, D.; Badloe, T.; Rho, J. Metamaterial-Based Radiative Cooling: Towards Energy-Free All-Day Cooling. *Energies* **2019**, *12*, 89. [CrossRef]
23. Solgi, E.; Hamedani, Z.; Fernando, R.; Skates, H.; Orji, N.E. A literature review of night ventilation strategies in buildings. *Energy Build.* **2018**, *173*, 337–352. [CrossRef]
24. Chohan, A.H.; Awad, J. Wind Catchers: An Element of Passive Ventilation in Hot, Arid and Humid Regions, a Comparative Analysis of Their Design and Function. *Sustainability* **2022**, *14*, 11088. [CrossRef]
25. Santamouris, M.; Kolokotsa, D. Passive cooling dissipation techniques for buildings and other structures: The state of the art. *Energy Build.* **2013**, *57*, 74–94. [CrossRef]
26. Sodha, M.S.; Sawhney, R.L.; Deshmukh, M.K. Energy conservation in large air-conditioned buildings: Use of evaporative roof cooling in hot and dry climates. *Int. J. Energy Res.* **1989**, *13*, 179–192. [CrossRef]
27. Boukhanouf, R.; Amer, O.; Ibrahim, H.; Calautit, J. Design and performance analysis of a regenerative evaporative cooler for cooling of buildings in arid climates. *Build. Environ.* **2018**, *142*, 1–10. [CrossRef]
28. Suichi, T.; Ishikawa, A.; Hayashi, Y.; Tsuruta, K. Performance limit of daytime radiative cooling in warm humid environment. *AIP Adv.* **2018**, *8*, 055124. [CrossRef]
29. Li, Z.; Chen, Q.; Song, Y.; Zhu, B.; Zhu, J. Fundamentals, Materials, and Applications for Daytime Radiative Cooling. *Adv. Mater. Technol.* **2020**, *5*, 1901007. [CrossRef]
30. Goldstein, E.A.; Raman, A.P.; Fan, S. Sub-ambient non-evaporative fluid cooling with the sky. *Nat. Energy* **2017**, *2*, 17143. [CrossRef]
31. Smith, G.; Gentle, A. Radiative cooling: Energy savings from the sky. *Nat. Energy* **2017**, *2*, 17142. [CrossRef]
32. Feng, C.; Yang, P.; Liu, H.; Mao, M.; Liu, Y.; Xue, T.; Fu, J.; Cheng, T.; Hu, X.; Fan, H.J.; et al. Bilayer porous polymer for efficient passive building cooling. *Nano Energy* **2021**, *85*, 105971. [CrossRef]
33. Xu, L.; Sun, D.-W.; Tian, Y.; Fan, T.; Zhu, Z. Nanocomposite hydrogel for daytime passive cooling enabled by combined effects of radiative and evaporative cooling. *Chem. Eng. J.* **2023**, *457*, 141231. [CrossRef]
34. Li, J.; Wang, X.; Liang, D.; Xu, N.; Zhu, B.; Li, W.; Yao, P.; Jiang, Y.; Min, X.; Huang, Z.; et al. A tandem radiative/evaporative cooler for weather-insensitive and high-performance daytime passive cooling. *Sci. Adv.* **2022**, *8*, eabq0411. [CrossRef]
35. Sun, Y.; Ji, Y.; Javed, M.; Li, X.; Fan, Z.; Wang, Y.; Cai, Z.; Xu, B. Preparation of Passive Daytime Cooling Fabric with the Synergistic Effect of Radiative Cooling and Evaporative Cooling. *Adv. Mater. Technol.* **2022**, *7*, 2100803. [CrossRef]
36. Fang, Y.; Zhao, X.; Chen, G.; Tat, T.; Chen, J. Smart polyethylene textiles for radiative and evaporative cooling. *Joule* **2021**, *5*, 752–754. [CrossRef]
37. Leroy, A.; Bhatia, B.; Kelsall, C.C.; Castillejo-Cuberos, A.; Di Capua, H.M.; Zhao, L.; Zhang, L.; Guzman, A.M.; Wang, E.N. High-performance subambient radiative cooling enabled by optically selective and thermally insulating polyethylene aerogel. *Sci. Adv.* **2019**, *5*, eaat9480. [CrossRef]
38. He, R.; Liao, Y.; Huang, J.; Cheng, T.; Zhang, X.; Yang, P.; Liu, H.; Liu, K. Radiant air-conditioning with infrared transparent polyethylene aerogel. *Mater. Today Energy* **2021**, *21*, 100800. [CrossRef]
39. Pu, S.; Fu, J.; Liao, Y.; Ge, L.; Zhou, Y.; Zhang, S.; Zhao, S.; Liu, X.; Hu, X.; Liu, K.; et al. Promoting Energy Efficiency via a Self-Adaptive Evaporative Cooling Hydrogel. *Adv. Mater.* **2020**, *32*, 1907307. [CrossRef] [PubMed]
40. Sartori, E. Convection coefficient equations for forced air flow over flat surfaces. *Sol. Energy* **2006**, *80*, 1063–1071. [CrossRef]
41. Mandal, J.; Fu, Y.; Overvig, A.C.; Jia, M.; Sun, K.; Shi, N.N.; Zhou, H.; Xiao, X.; Yu, N.; Yang, Y. Hierarchically porous polymer coatings for highly efficient passive daytime radiative cooling. *Science* **2018**, *362*, 315–319. [CrossRef]